Title

Quantitative susceptibility mapping (QSM) as a means to monitor cerebral hematoma treatment

Journal

Journal of Magnetic Resonance Imaging, 48(4)

ISSN

1053-1807

Authors

Zhang, Yuyao
Wei, Hongjiang
Sun, Yawen
et al.

Publication Date

2018-10-01

DOI

10.1002/jmri.25957

Peer reviewed

HHS Public Access

Author manuscript

J Magn Reson Imaging. Author manuscript; available in PMC 2019 October 01.

Published in final edited form as:

J Magn Reson Imaging. 2018 October ; 48(4): 907–915. doi:10.1002/jmri.25957.

Quantitative Susceptibility Mapping (QSM) As a Means to Monitor Cerebral Hematoma Treatment

Yuyao Zhang, PhD[1,#], **Hongjiang Wei, PhD**[1,#], **Yawen Sun, MD**[2], **Matthew J. Cronin, PhD**[1], **Naying He, MD, PhD**[3], **Jianrong Xu, MD, PhD**[2], **Yan Zhou, MD, PhD**[2], and **Chunlei Liu, PhD**[1,4]

[1]Department of Electrical Engineering and Computer Sciences, University of California, Berkeley, CA, USA

[2]Department of Radiology, Ren Ji Hospital, School of Medicine, Shanghai Jiao Tong University, Shanghai, China

[3]Department of Radiology, Rui Jin Hospital, School of Medicine, Shanghai Jiao Tong University, Shanghai, China

[4]Helen Wills Neuroscience Institute, University of California, Berkeley, CA, USA

Abstract

Background—Quantitative susceptibility mapping (QSM) offers a consistent hemorrhage volume measurement independent of imaging parameters.

Purpose—To investigate magnetic susceptibility of intracerebral hemorrhage (ICH) as a quantitative measurement for monitoring treatment in hematoma patients.

Study Type—Prospective

Population—26 patients with acute ICH were recruited and were enrolled in treatment including surgery or medication (Mannitol) for one week.

Field Strength/Sequence—3D Gradient Echo sequence at 3.0T.

Assessment—The hematoma volumes on CT and QSM were calculated and used for correlation analysis. Magnetic susceptibility changes from pre- to post-treatment were calculated and compared to the NIH stroke scale (NIHSS) measure of neurological deficit for each patient.

Statistical Tests—Mean susceptibility values were calculated over each ROI. A one-sample t-test was used to assess the changes of total volumes and mean magnetic susceptibility of ICH identified between pre- and post-treatment images ($P<0.05$ was considered significant) and the Bland-Altman analysis with 95% limits of agreement (average difference, ± 1.96 SD of the difference). Regression of volume measurements on QSM versus CT and fitted linear regression of mean susceptibility versus CT signal intensity for hematoma regions were conducted in all patients.

Correspondence Address: Chunlei Liu, Ph.D., Department of Electrical Engineering and Computer Sciences, and the Helen Wills Neuroscience Institute at the University of California, Berkeley., 505 Cory Hall, Berkeley, CA 94720, USA., Phone: (510)664 7596, chunlei.liu@berkeley.edu.

[#]These authors contributed equally to this work

Results—Good correlation was found between hemorrhage volumes calculated from CT and QSM (CT volume = 0.94*QSM volume, r = 0.98). Comparison of QSM pre- and post-treatment showed that the mean ICH volume was reduced by a statistically insignificant amount from 5.74 cm^3 to 5.45 cm^3 (P = 0.21), while mean magnetic susceptibility was reduced significantly from 0.48 ppm to 0.38 ppm (P = 0.004). A significant positive association was found between changes in magnetic susceptibility values and NIHSS following hematoma treatment (P <0.01).

Data Conclusions—QSM in hematoma assessment, as compared with CT, offers a comparably accurate volume measurement, however, susceptibility measurements may enable improved monitoring of ICH treatment compared to volume measurements alone.

Keywords

Computed tomography; hematoma volume; intracerebral hemorrhage; magnetic resonance imaging; quantitative susceptibility mapping

Introduction

Intracerebral hemorrhage (ICH) is a potentially devastating neurological injury representing 10 – 15% of stroke cases in the world each year (1). Timely identification and management of this condition remain a challenge for clinicians as numerous factors can present obstacles to achieving good functional outcomes. Most of the current management guidelines do exist on medical evidence and consensus and these provide a framework for care (2). ICH remains a disease treated usually with pharmaceuticals to relieve the pressure from accumulation of blood (3).

In the acute setting, predictors of 30-day mortality include hematoma size, hematoma expansion, older patient age, coma, and hematoma location (4,5). Currently, greater than one-third of patients with ICH will not survive and only twenty percent of patients will regain functional independence (1). This high rate of morbidity and mortality has prompted continued investigation of tools for the accurate localization and quantitative characterization of ICH to diagnose and evaluate the severity of ICH. A previous study had reported QSM changes occurred in one subject when surgical intervention was involved (6). Therefore, development of effective imaging biomarkers for monitoring of treatment has the potential to mitigate the economic and social burden of ICH.

Magnetic resonance imaging (MRI) is increasingly being advocated as a comprehensive multimodal imaging approach for patients presenting with acute stroke symptoms (7). Patients frequently undergo both MRI and computed tomography (CT) scanning as part of routine clinical care and research protocols. However, CT delivers potential risks of high dose of radiation to the human body. Gradient echo (GRE) MRI has been shown to be more sensitive than CT for detecting intracerebral hemorrhage (8–10). However, hypointensity in T2*-weighted GRE magnitude images is known to overestimate hematoma volume as these images suffer from susceptibility artifacts that are highly dependent on imaging parameters, such as field strength, voxel size and echo time. In contrast, quantitative susceptibility mapping (QSM) (9,11–14) based on GRE phase data can provide an accurate measurement of the hemorrhage volumes by removing blooming artifacts inherent in traditional T2*-

weighted imaging (15). QSM offers excellent image contrast by computing the spatial distribution of the underlying source of the phase contrast, i.e. magnetic susceptibility (16–25). Since iron is the major contributor to the magnetic susceptibility of hemorrhage, the highly paramagnetic blood lesions exhibit clear delineation within the surrounding relatively diamagnetic brain tissues. Thus, QSM may prove to be especially helpful when surgical treatments are applied to remove hemorrhagic fluid surrounded by soft tissues.

Additionally, hematoma treatment presents a unique challenge due to different hemorrhagic products and non-uniform iron deposition within individual lesions. The blood degradation in hemorrhage has rarely been characterized on conventional MRI images. During complex blood degradation in hemorrhage, hemoglobin changes through several forms (26). The magnetic susceptibility progressively increases from slightly diamagnetic relative to cerebrospinal fluid (CSF) in oxyhemoglobin to paramagnetic in deoxyhemoglobin, methemoglobin and hemosiderin (27,28). The sensitivity of QSM to such changes allows quantification of changes in the composition of the hematoma using MRI (28), especially at the hyperacute and acute stages where timely treatment is critically important. It may be used to precisely assess treatment outcomes, providing useful quantitative information in hemorrhage patient management. Previous studies have shown that susceptibility changes in one subject when surgical intervention was performed (6). Therefore, there is an ongoing need to establish a correlation between magnetic susceptibility of hemorrhages and clinical measures.

In the current study, we sought to determine if the mean magnetic susceptibility pre- and post-treatment in ICH in QSM can be used as a biomarker to monitor treatment.

Materials and Methods

Patients

The study protocol was reviewed and approved by the Institutional Review Board and written informed consent was obtained from all participants prior to enrollment in the study. Twenty-six patients with acute ICH (58 ± 15.1 years; 17 men, 9 women) were recruited from September 21, 2014, to March 01, 2015. All participants underwent imaging with MRI and CT scans as routine clinical ICH diagnosis. All hospitalized patients were actively enrolled in treatment including surgery and medication to decrease intracranial pressure and hemostatic therapy. After their conditions stabilized, post-treatment CT and MRI scans were performed on twenty-one patients. The interval between the pre- and post-treatment scans ranged from 5 to 8 days. Five patients were discharged before the post-treatment scans. Scores on the National Institute of Health Stroke Scale (NIHSS) (29) were measured for each patient both pre- and post-treatment. All patients recovered and were discharged a few days after the post-treatment scans. Treatment details for individual patients are listed in Table 1.

MR imaging and Data reconstruction

All patients underwent brain MR examination on a 3 T scanner (Signa HDxt, GE Healthcare, Waukesha, WI) equipped with an 8-channel head coil. Phase images with

whole-brain coverage were acquired using a standard flow-compensated 3D SPGR sequence with the following parameters: $TE_1/\Delta TE/TE_{16}$ = 3.16/2.42/39.5 ms, TR = 43 ms, FA = 12°, FOV = 220×220×132 mm^3, matrix size = 256×256×66. The raw phase was processed by Laplacian-based phase unwrapping (30) and the normalized phase was calculated as $\frac{\sum_{i=8}^{n}\varphi_i}{\gamma\mu_0 H_0 \sum_{i=8}^{n} TE_i}$ where n is the number of echoes. Note that i≥8 (TE>20ms) since previous study has reported that magnetic susceptibility in hematoma was independence of TE for echo times longer than 20 msec (15). The normalized background phase was removed by V-SHARP (31). QSM images were calculated using STAR-QSM (streaking artifact reduced quantitative susceptibility mapping) (32–34).

Data Analysis

The hemorrhage volume was obtained by semi-automated level set segmentation using MIPAV (Medical Image Processing, Analysis, and Visualization, NIH). Lesions were segmented using regions of interest (ROIs) across multiple slices (3D ROI) on CT and QSM. κ analysis was performed to assess the reliability of volume measurement between two independent radiologists (Y.Z., 20 years of experience; J.X., 33 years of experience). To access the sharpness between hematoma lesions and surrounding tissues, the line profiles were drawn on QSM images and tissue phase maps.

Statistical analysis

κ statistics (35) were interpreted as indicating poor (κ, <0), slight (0<κ<0.2), fair (0.21<κ<0.4), moderate (0.41<κ<0.6), substantial (0.61<κ<0.8), and almost perfect (0.81<κ<1.0) observer agreement (36). Mean susceptibility values were calculated over each ROI, and normalized relative to mean susceptibility of the cerebrospinal fluid (CSF) in the lateral ventricles without evidence of hemorrhages. A paired sample t-test was used to assess the changes of total volumes and mean magnetic susceptibility of ICH identified between pre- and post-treatment images (P<0.05 was considered significant) and the Bland-Altman analysis with 95% limits of agreement (average difference, ± 1.96 SD of the difference). Regression of volume measurements on QSM versus CT and fitted linear regression of mean susceptibility versus CT signal intensity for hematoma regions were conducted in all patients.

Results

Examples of T2*-weighted magnitude, R2*, QSM and tissue phase images of an ICH patient are shown in Fig. 1. The apparent size of the hematoma on T2* weighted magnitude images increased substantially relative to the boundary defined on the image at TE_1 = 3.2 ms as blooming artifacts increased with echo time (Fig. 1A). As a consequence, the boundary between the hematoma and surrounding tissues may be inaccurately defined on such images and on R2* image (Fig. 1B). The phase image makes the boundary definition more difficult since the non-local properties of the phase image as shown in Fig. 1C. QSM offers a cleaner and sharper definition of boundaries between the hematoma lesion and surrounding tissues as pointed by white arrows in Fig. 1D and by dash lines in Fig. S1. In addition, the

geometric shape of the hematoma revealed by susceptibility maps at the longest TE=39.5 ms remains highly consistent with that at TE = 3.2ms.

The two radiologists had high agreement on measured hematoma volumes in all patients. The interobserver reliability was 95.4% according to κ analysis. Fig. 2 shows representative CT and QSM images pre- and post-treatment in a 67-year-old male patient. The boundary of the hematoma lesion on the corresponding axial location on CT and QSM are similar and are indicated by the red curves. Overall, mean hemorrhage volume was 5.24 cm^3 measured on CT and 5.6 cm^3 on QSM. A linear relationship defined by CT volume = 0.94 × QSM volume (r=0.98) was derived from all pre- and post-treatment images. Fig. 2D showed good agreement in volume measurement between CT and QSM images. In addition, the correspondence between paramagnetic susceptibility of hematoma regions in QSM and high Hounsfield unit (HU) values in CT is supported by a linear correlation (r=0.37, P=0.016) (Fig. S2A in the supplementary material). No significant correlation was found between volume measurement and estimated magnetic susceptibility (Fig. S2B).

Fig. 3 shows the hematoma volume and susceptibility change following treatment in a 15-year-old male patient. The hemorrhage size was 4.7 cm^3 and 3.31 cm^3 measured on QSM images of pre- and post-treatment, respectively. The corresponding mean magnetic susceptibility values were 0.28 ppm and 0.10 ppm. Both volume and magnetic susceptibility decreased in response to the treatment. Fig. 4 shows another representative case in a 55-year-old man, the pre-treatment hematoma volume was 7.65 cm^3 and post-treatment volume was 7.53 cm^3 measured on QSM images. However, the corresponding mean magnetic susceptibility values were 0.79 ppm to 0.64 ppm. Moreover, the hematoma regions exhibit a heterogeneous distribution of magnetic susceptibility with more paramagnetic susceptibility values in the center than at the boundaries as highlighted in the colormaps in Fig. 3 and 4.

As shown in Fig. 5A, QSM-derived total volume did not decrease significantly between pre- and post-treatment scans (P>0.5). However, considerable changes were found in the magnetic susceptibility following the treatment (Fig. 5B). Figs. 5A (bottom) and B (bottom), illustrate the changes in the total volume and mean magnetic susceptibility (from pre- to post-treatment scans), respectively, for each individual patient. The negative changes indicate that the total volumes of the hemorrhages slightly decreased in all twenty one patients (Fig. 5A bottom). In all but one patient, the mean magnetic susceptibility also decreased. One patient showed slightly increased mean magnetic susceptibility after treatment (Fig. 5B bottom). A significant change of mean magnetic susceptibility across all patients was found between pre- and post-treatment imaging (P=0.004) but no significant change was found in the QSM-derived total volume (P=0.21). NIHSS measured on each individual patient is listed in Table 1, and NIHSS changes following the treatment (post-treatment – pre-treatment) are shown in Fig. 5C.

No significant correlation was found between hematoma volume and NIHSS changes following treatment as shown in Fig. 6A&B. No significant correlation was found between volume changes and QSM values changes (Fig. S3 in the supplementary material). No significant correlation was found between CT values changes and NIHSS changes as shown in Fig. S4. However, significant positive correlations were observed between NIHSS

changes and QSM values changes (Fig. 6C, r = 0.8, P < 0.001) or QSM values percentage changes (Fig. 6D, r = 0.71, P = 0.003).

Discussion

The current study demonstrates that QSM offers excellent image contrast and is more sensitive than CT in the detection of hemorrhages. In addition, the volume of the hematomas determined on CT and QSM images was compared. Comparison of mean magnetic susceptibility between pre- and post-treatment was also conducted in hematoma lesions and was correlated with corresponding NIHSS changes. This study led to several unique findings: 1) a high correlation of volume measurement on CT and QSM with highly linear relationship; 2) magnetic susceptibility decreased significantly following treatment while no significant changes were found in hematoma volume; 3) the susceptibility values changes following treatment were significantly positively correlated with NIHSS changes.

Robust volume measurement is important on an individual-patient level because hematoma size correlates with hematoma growth and is associated with early neurological deterioration and treatment outcome (37). However, the apparent size of hemorrhage lesions on magnitude GRE MRI and CT are not equal because of the underlying differences in the imaging modalities. Previous studies on hematoma have shown that CT volume = 0.8* GRE volume (38). QSM, which is insensitive to the parameter-dependent blooming artifacts seen in GRE magnitude images, provides a reliable measurement that is independent of imaging parameters to reveal the tissue properties. Wang et al (15) measured the hematoma volume using QSM and showed magnitude volume/QSM volume = 1.24 (15). Our results show a strong correlation between lesion volume measured on CT and QSM with a highly linear relationship. The relative underestimation of the volume measured on CT compared to that measured on QSM is caused by the insensitivity of CT to the presence of small hemorrhage lesions. This suggests that QSM offers a more reliable measurement in hematoma volume than CT.

In the patients who underwent the post-treatment imaging, mean susceptibility in the hemorrhages derived from QSM decreased following the treatment. While this result suggests that QSM is a promising means of measuring treatment efficacy although the aging of the hemorrhagic lesion may be a potentially confounding issue. Previous studies observed that the susceptibility values monotonically increased with time in an in vitro human blood phantom (28). However, another study showed that the susceptibility decreased from acute to late subacute ICH (27). The susceptibility changes following the treatment may also be admixed with changes related to the natural evolution of hematoma susceptibility over time. However, a recent study on monitoring microhemorrhage magnetic susceptibility changes reported that the susceptibility decreased over time: −0.1 ± 0.14 ppb per day (39). Therefore, the observed susceptibility value change varying from −10 ppb up to −260 ppb are mainly contributed to treatments. We showed, for the first time to our knowledge, that the magnetic susceptibility of hemorrhages decreases following the hematoma treatment. The measured magnetic susceptibility reduction following the hematoma treatment reflects a lower concentration of methemoglobin. This finding may indicate the clearance of methemoglobin

by effective treatments such as surgical drainage or medications significantly dilute the concentration of methemoglobin.

Because iron in hemorrhage is the most concentrated in the center, the smaller the volume drawn, the larger the mean susceptibility is. Therefore, the volume of the ICH is negatively correlated with the mean magnetic susceptibility for a specific lesion. Sun et al. (40) reported that the mean susceptibility of ICH over a 2D ROI was up to1.8 ppm which is almost as double as our measurements. However, Chang et al. (27) measured the susceptibility values (0.5–0.8 ppm) of blood clot phantom over a 3D ROI in the first 4 days, which is consistent with our measurements on ICH patients at acute stage. Therefore, it is likely that a subjective bias on the manually segmentation of the hematoma volumes on a single 2D slice or over a 3D volume caused the discrepancy.

Further correlation of susceptibility values changes with NIHSS changes suggests that QSM is an effective means to monitor treatment. However, a good correlation between magnetic susceptibility and other clinical measures needs to be established in the future. In particular, more efforts should make to investigate the magnetic susceptibility changes specific to different treatments such as surgical drainage or medications, for certain hematomas.

In this study, a major limitation consists of a limited number of patients who underwent follow-up imaging examinations. In future studies, this method will need to be replicated in a larger patient population. Furthermore, by correlating hematoma with regional brain volumes, abnormalities such as fiber discontinuities or hyperintensities on T2-weighted fluid attenuation inversion recovery images will facilitate the investigation of the hematoma.

In summary, we found that QSM-derived magnetic susceptibility of hematoma decreased following treatment while volume did not, suggesting a more effective means to monitor hematoma treatment. Characterization of magnetic susceptibility of hematoma lesions, brain tissue, and vasculature may allow better understanding and management of hematoma expansion and would be important in developing and applying hemorrhage therapy. QSM offers a more direct way to quantify the magnetic susceptibility of blood products, may become an essential part of a hemorrhage MRI protocol and the method of choice clinically to monitor the hematoma treatment.

Supplementary Material

Refer to Web version on PubMed Central for supplementary material.

Acknowledgments

This study was supported in part by the National Institutes of Health through grants NIMH R01MH096979. The National Natural Science Foundation of China (No. 81571650), Shanghai Municipal Education Commission-Gaofeng Clinical Medicine Grant Support (No. 20172013), Shanghai Science and Technology Committee Medical Guide Project (No. 17411964300), Medical Engineering Cross Research Foundation of Shanghai Jiao Tong University (No. YG2017QN47), and Research Seed Fund of Ren Ji Hospital, School of Medicine, Shanghai Jiao Tong University (RJZZ17-016).

References

1. Sahni R, Weinberger J. Management of intracerebral hemorrhage. Vascular health and risk management. 2007; 3(5):701. [PubMed: 18078021]
2. Broderick JP, Adams HP, Barsan W, et al. Guidelines for the management of spontaneous intracerebral hemorrhage. Stroke. 1999; 30(4):905–915. [PubMed: 10187901]
3. Mayer SA, Rincon F. Treatment of intracerebral haemorrhage. The Lancet Neurology. 2005; 4(10): 662–672. [PubMed: 16168935]
4. Broderick JP, Brott TG, Duldner JE, Tomsick T, Huster G. Volume of intracerebral hemorrhage. A powerful and easy-to-use predictor of 30-day mortality. Stroke. 1993; 24(7):987–993. [PubMed: 8322400]
5. Tuhrim S, Dambrosia JM, Price TR, et al. Intracerebral hemorrhage: external validation and extension of a model for prediction of 30-day survival. Annals of neurology. 1991; 29(6):658–663. [PubMed: 1842899]
6. Tan H, Zhang L, Mikati AG, et al. Quantitative susceptibility mapping in cerebral cavernous malformations: clinical correlations. American Journal of Neuroradiology. 2016; 37(7):1209–1215. [PubMed: 26965464]
7. Patel MR, Edelman RR, Warach S. Detection of hyperacute primary intraparenchymal hemorrhage by magnetic resonance imaging. Stroke. 1996; 27(12):2321–2324. [PubMed: 8969800]
8. Liu S, Buch S, Chen Y, et al. Susceptibility-weighted imaging: current status and future directions. NMR in Biomedicine. 2017; 30(4)
9. Haacke EM, Liu S, Buch S, Zheng W, Wu D, Ye Y. Quantitative susceptibility mapping: current status and future directions. Magnetic resonance imaging. 2015; 33(1):1–25. [PubMed: 25267705]
10. Kidwell CS, Chalela JA, Saver JL, et al. Comparison of MRI and CT for detection of acute intracerebral hemorrhage. Jama. 2004; 292(15):1823–1830. [PubMed: 15494579]
11. Wang Y, Liu T. Quantitative susceptibility mapping (QSM): decoding MRI data for a tissue magnetic biomarker. Magnetic resonance in medicine. 2015; 73(1):82–101. [PubMed: 25044035]
12. Liu C, Wei H, Gong N-J, Cronin M, Dibb R, Decker K. Quantitative susceptibility mapping: contrast mechanisms and clinical applications. Tomography: a journal for imaging research. 2015; 1(1):3.
13. Deistung A, Schweser F, Reichenbach JR. Overview of quantitative susceptibility mapping. NMR in Biomedicine. 2017; 30(4)
14. Wei H, Xie L, Dibb R, et al. Imaging whole-brain cytoarchitecture of mouse with MRI-based quantitative susceptibility mapping. NeuroImage. 2016; 137:107–115. [PubMed: 27181764]
15. Wang S, Lou M, Liu T, Cui D, Chen X, Wang Y. Hematoma volume measurement in gradient echo MRI using quantitative susceptibility mapping. Stroke. 2013; 44(8):2315–2317. [PubMed: 23704111]
16. Bilgic B, Pfefferbaum A, Rohlfing T, Sullivan EV, Adalsteinsson E. MRI estimates of brain iron concentration in normal aging using quantitative susceptibility mapping. Neuroimage. 2012; 59(3): 2625–2635. [PubMed: 21925274]
17. Wei H, Gibbs E, Zhao P, et al. Susceptibility tensor imaging and tractography of collagen fibrils in the articular cartilage. Magnetic resonance in medicine. 2017; 78(5):1683–1690. [PubMed: 28856712]
18. Wehrli FW, Fan AP, Rodgers ZB, Englund EK, Langham MC. Susceptibility-based time-resolved whole-organ and regional tissue oximetry. NMR in Biomedicine. 2017; 30(4)
19. Dibb R, Xie L, Wei H, Liu C. Magnetic susceptibility anisotropy outside the central nervous system. NMR in Biomedicine. 2016
20. Langkammer C, Schweser F, Krebs N, et al. Quantitative susceptibility mapping (QSM) as a means to measure brain iron? A post mortem validation study. Neuroimage. 2012; 62(3):1593–1599. [PubMed: 22634862]
21. Li X, Zijl P. Mean magnetic susceptibility regularized susceptibility tensor imaging (MMSR-STI) for estimating orientations of white matter fibers in human brain. Magnetic resonance in medicine. 2014; 72(3):610–619. [PubMed: 24974830]

22. Liu C, Li W, Tong KA, Yeom KW, Kuzminski S. Susceptibility-weighted imaging and quantitative susceptibility mapping in the brain. Journal of Magnetic Resonance Imaging. 2015; 42(1):23–41. [PubMed: 25270052]
23. Fan AP, Govindarajan ST, Kinkel RP, et al. Quantitative oxygen extraction fraction from 7-Tesla MRI phase: reproducibility and application in multiple sclerosis. Journal of Cerebral Blood Flow & Metabolism. 2015; 35(1):131–139. [PubMed: 25352043]
24. Klohs J, Deistung A, Schweser F, et al. Detection of cerebral microbleeds with quantitative susceptibility mapping in the ArcAbeta mouse model of cerebral amyloidosis. Journal of Cerebral Blood Flow & Metabolism. 2011; 31(12):2282–2292. [PubMed: 21847134]
25. Bao L, Li X, Cai C, Chen Z, van Zijl PC. Quantitative Susceptibility Mapping Using Structural Feature Based Collaborative Reconstruction (SFCR) in the Human Brain. IEEE transactions on medical imaging. 2016; 35(9):2040–2050. [PubMed: 27019480]
26. Keep RF, Hua Y, Xi G. Intracerebral haemorrhage: mechanisms of injury and therapeutic targets. The Lancet Neurology. 2012; 11(8):720–731. [PubMed: 22698888]
27. Chang S, Zhang J, Liu T, et al. Quantitative Susceptibility Mapping of Intracerebral Hemorrhages at Various Stages. Journal of Magnetic Resonance Imaging. 2015
28. Gho SM, Shin J, Kim MO, Kim DH. Simultaneous quantitative mapping of conductivity and susceptibility using a double-echo ultrashort echo time sequence: Example using a hematoma evolution study. Magnetic resonance in medicine. 2015
29. Lyden P, Brott T, Tilley B, et al. Improved reliability of the NIH Stroke Scale using video training. NINDS TPA Stroke Study Group. Stroke. 1994; 25(11):2220–2226. [PubMed: 7974549]
30. Basser PJ, Pierpaoli C. Microstructural and physiological features of tissues elucidated by quantitative-diffusion-tensor MRI. Journal of magnetic resonance. 2011; 213(2):560–570. [PubMed: 22152371]
31. Wu B, Li W, Guidon A, Liu C. Whole brain susceptibility mapping using compressed sensing. Magnetic resonance in medicine. 2012; 67(1):137–147. [PubMed: 21671269]
32. Wei H, Dibb R, Zhou Y, et al. Streaking artifact reduction for quantitative susceptibility mapping of sources with large dynamic range. NMR in Biomedicine. 2015; 28(10):1294–1303. [PubMed: 26313885]
33. Wei H, Dibb R, Decker K, et al. Investigating magnetic susceptibility of human knee joint at 7 tesla. Magnetic resonance in medicine. 2017; 78(5):1933–1943. [PubMed: 28097689]
34. Wei H, Zhang Y, Gibbs E, Chen NK, Wang N, Liu C. Joint 2D and 3D phase processing for quantitative susceptibility mapping: application to 2D echo-planar imaging. NMR in Biomedicine. 2016
35. Hanafi M, Kiers HA. Analysis of K sets of data, with differential emphasis on agreement between and within sets. Computational Statistics & Data Analysis. 2006; 51(3):1491–1508.
36. Kundel HL, Polansky M. Measurement of observer agreement 1. Radiology. 2003; 228(2):303–308. [PubMed: 12819342]
37. Davis S, Broderick J, Hennerici M, et al. Hematoma growth is a determinant of mortality and poor outcome after intracerebral hemorrhage. Neurology. 2006; 66(8):1175–1181. [PubMed: 16636233]
38. Burgess RE, Warach S, Schaewe TJ, et al. Development and validation of a simple conversion model for comparison of intracerebral hemorrhage volumes measured on CT and gradient recalled echo MRI. Stroke. 2008; 39(7):2017–2020. [PubMed: 18483414]
39. Liu W, Soderlund K, Senseney JS, et al. Imaging cerebral microhemorrhages in military service members with chronic traumatic brain injury. Radiology. 2015; 278(2):536–545. [PubMed: 26371749]
40. Sun H, Kate M, Gioia LC, Emery DJ, Butcher K, Wilman AH. Quantitative susceptibility mapping using a superposed dipole inversion method: application to intracranial hemorrhage. Magnetic resonance in medicine. 2016; 76(3):781–791. [PubMed: 26414757]

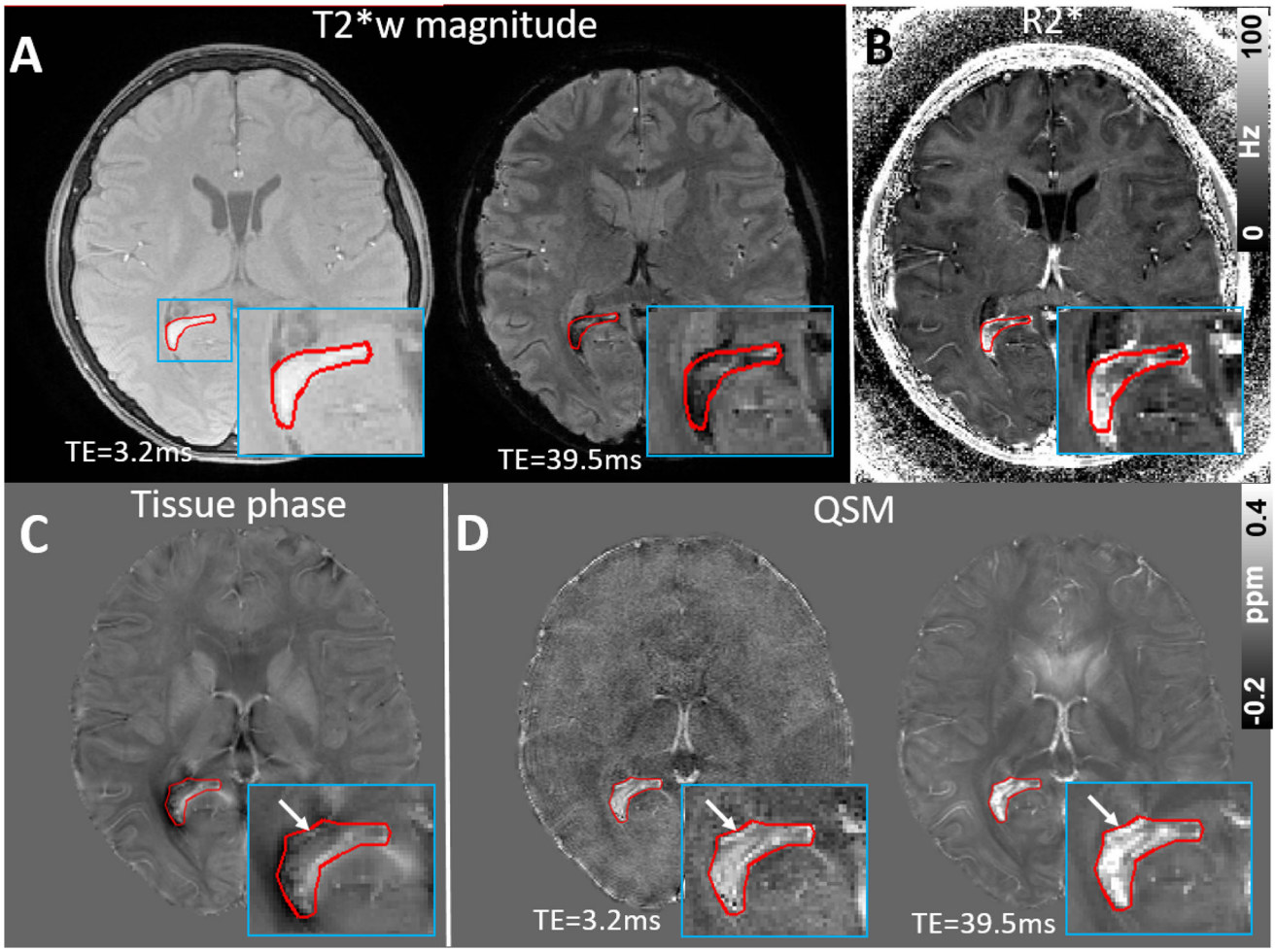

Figure 1.

A comparison of hematoma volume measurements on GRE magnitude, R2*, phase image, and QSM images in a representative ICH in a 15-year-old male. (A) The volume of the hemorrhage increased with echo time on GRE magnitude. (B) R2* image. (C). Phase image. (D) The hemorrhage volume stays consistent on QSM images at two representative echo times.

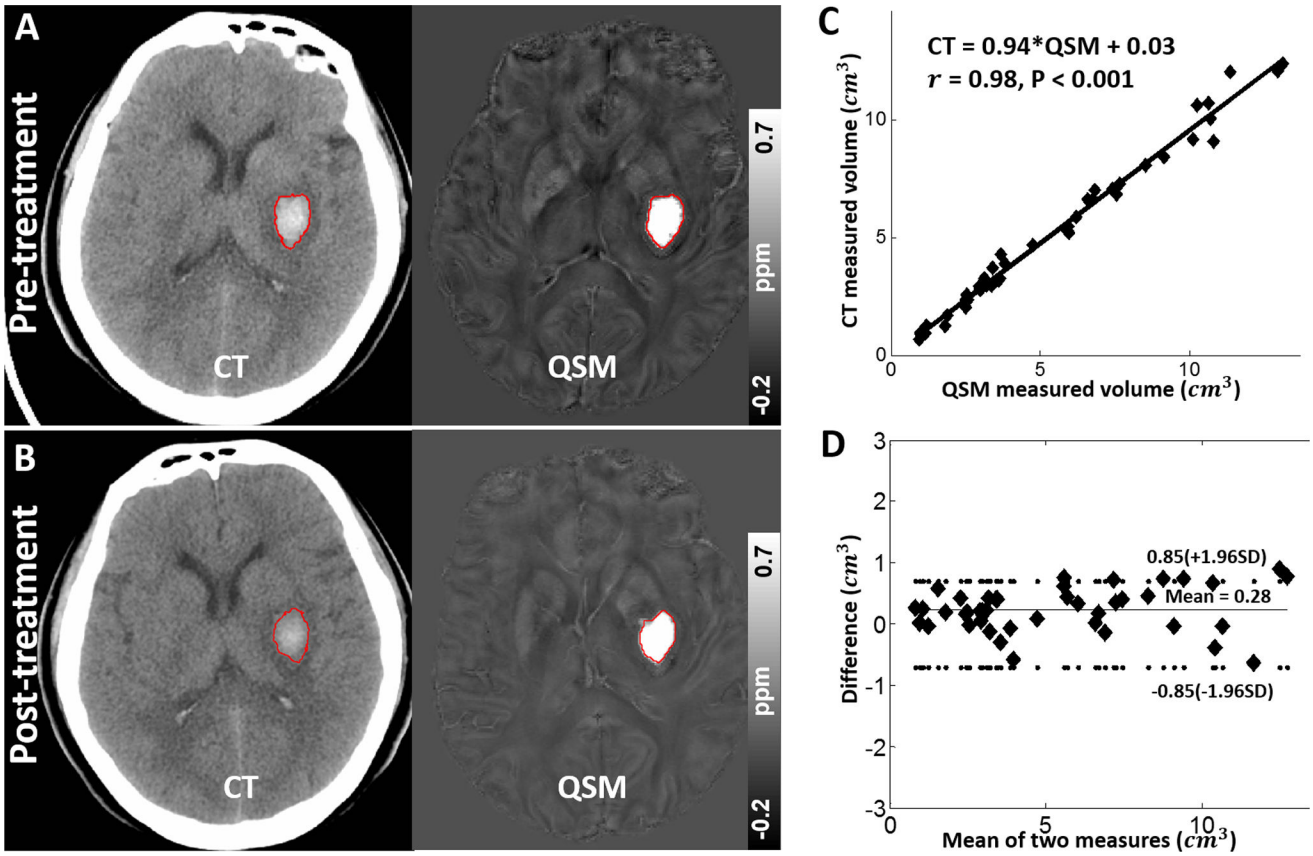

Figure 2.

(A) & (B) Comparison of QSM versus CT for hemorrhage volume measurement. (C) Regression of volume measurements on QSM versus CT in all patients. (D) Comparison analysis of volume measurement on CT versus QSM images using Bland-Altman plot.

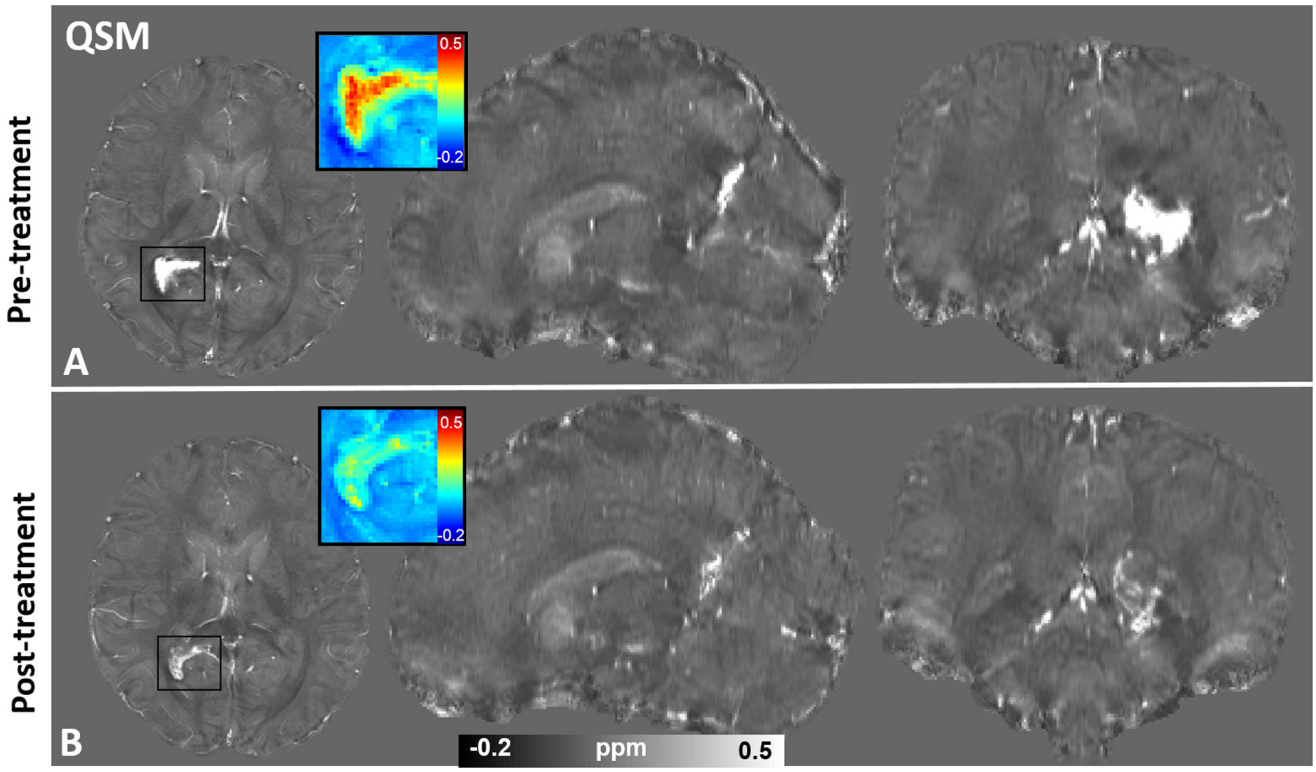

Figure 3.
Representative QSM images show that both volume and magnetic susceptibility decreased following treatment in a 15-year-old male patient.

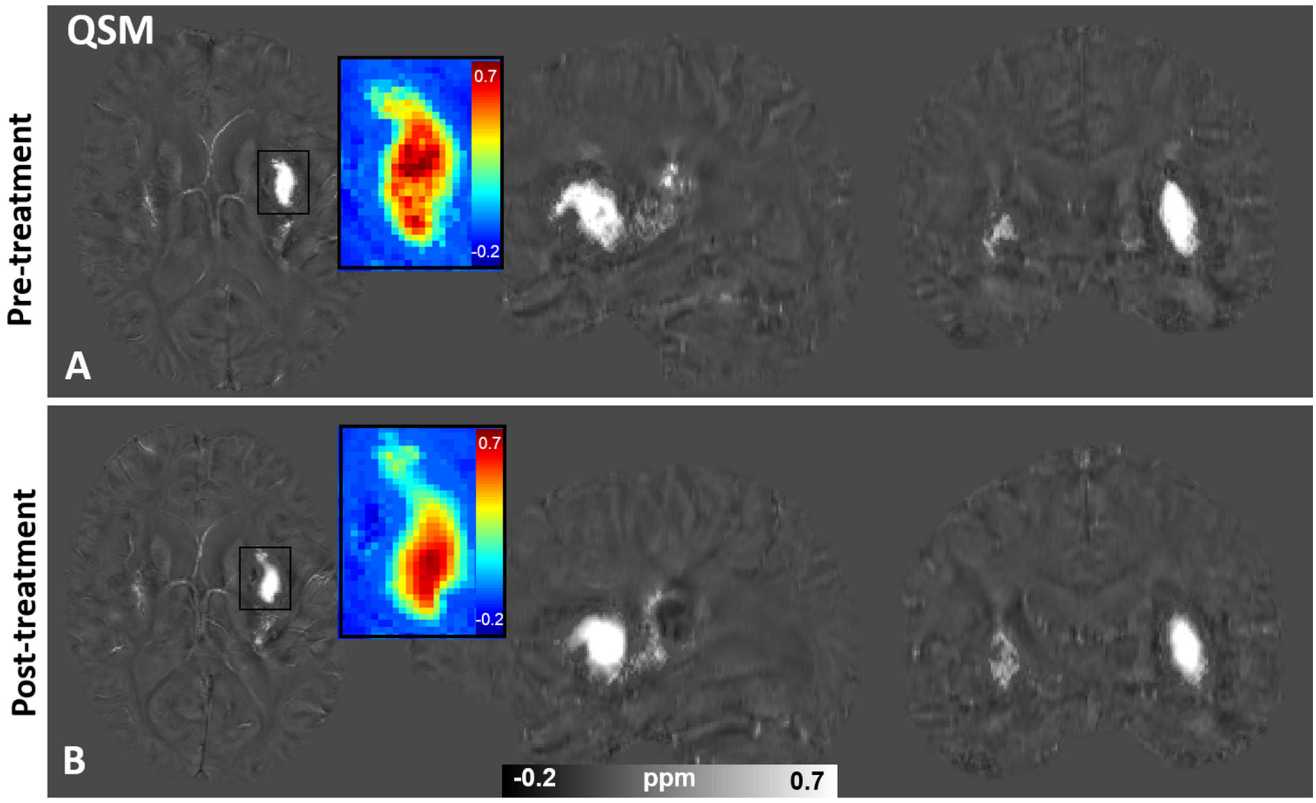

Figure 4.

Representative QSM images show that volume and magnetic susceptibility changes with treatment in a 55-year-old male patient.

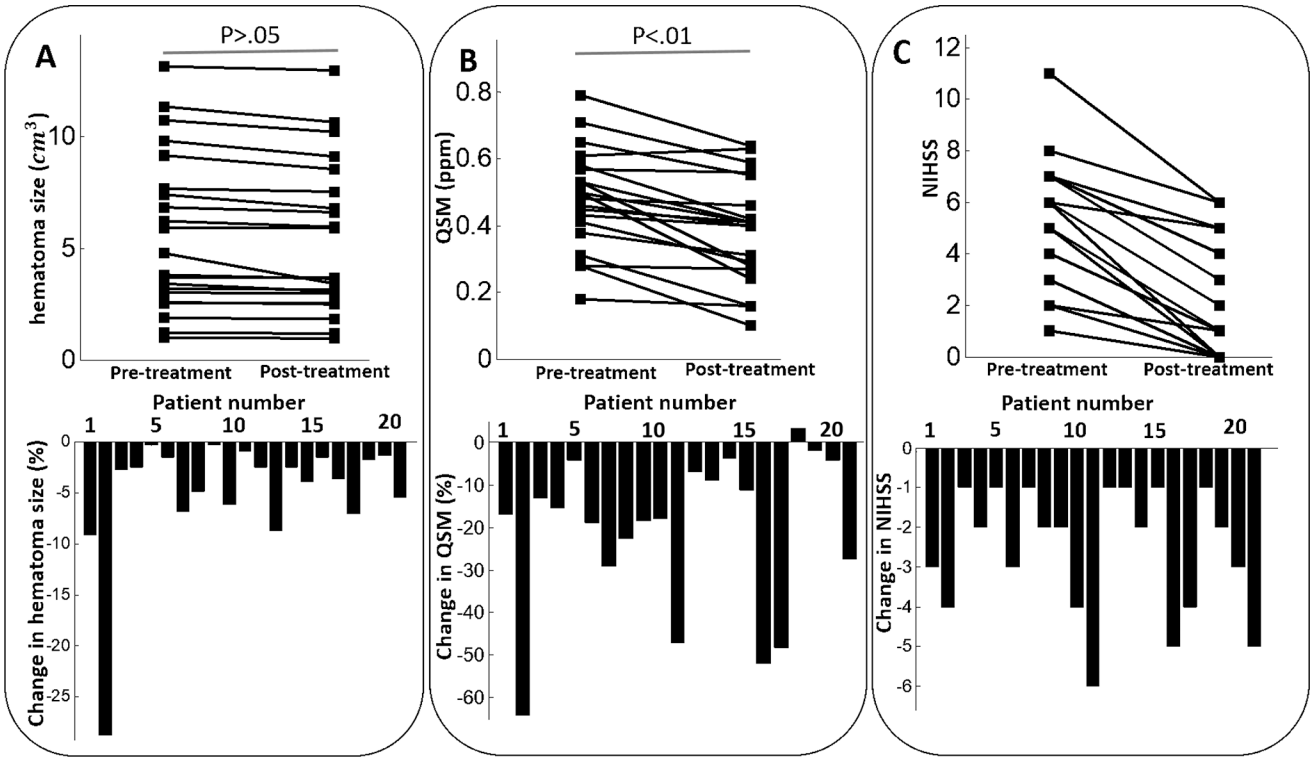

Figure 5.

(A) Top: total volume of hemorrhages in individual patients who underwent post-treatment imaging. Bottom: bar graph shows the relative changes in the total volume of hemorrhages (from pre- to post-treatment imaging) in individual patients. (B) Top: mean magnetic susceptibility of hemorrhages in individual patients who underwent post-treatment imaging; Bottom: bar graph shows the relative changes in mean magnetic susceptibility of hemorrhages (from pre- to post-treatment imaging) in individual patients. (C) Top: plot of the NIHSS of individual patients pre- and post-treatment. Bottom: bar graph shows the difference in NIHSS of individual patients pre- and post-treatment.

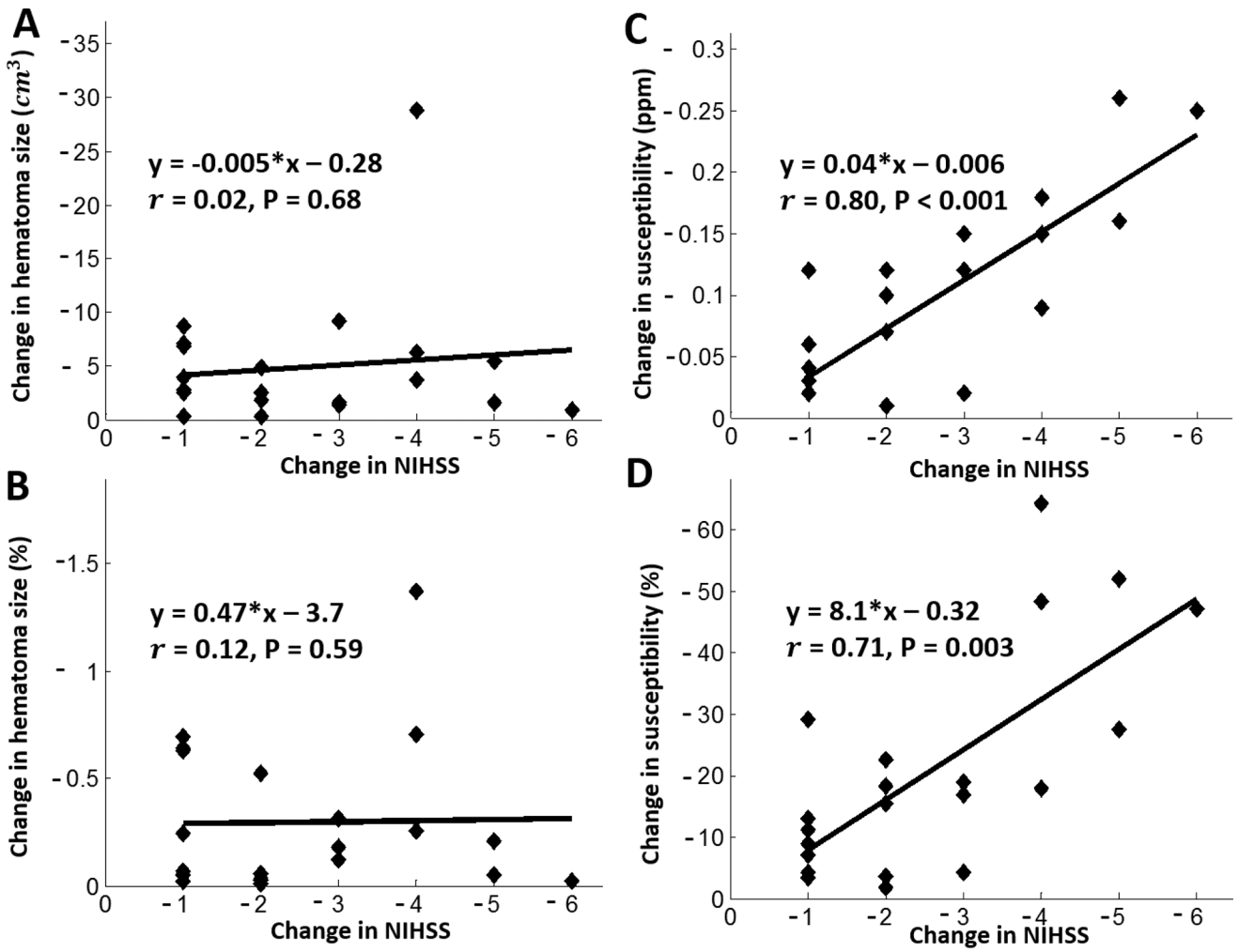

Figure 6.

Scatter plots and regression lines show the relationship between changes in NIHSS and in hematoma volume and in susceptibility values (post-treatment – pre-treatment). (A)&(B) No correlation was found between NIHSS changes and volume changes following treatment. (C)&(D) Significant correlation was found between NIHSS changes and susceptibility values changes (C, r = 0.8, P < 0.001) and susceptibility percentage changes (D, r = 0.71, P = 0.003).

Table 1

NIHSS on each individual patient pre- and post-treatment.

Case no.	Age/ Sex	ICH Location	Treatment	NIHSS (pre/post)	Case no.	Age/ Sex	ICH Location	Treatment	NIHSS (pre/post)
1	47/F	Putamen	Mannitol	4/1	12	65/M	Thalamus	Mannitol	6/5
2	15/M	Subcortex	Mannitol	7/3	13	49/M	Cerebellum	Mannitol	1/0
3	67/M	Putamen	Mannitol	1/0	14	60/M	Pons	Mannitol	2/0
4	63/M	Putamen	Surgery	8/6	15	84/M	Subcortex	Surgery	2/1
5	43/F	Putamen	Alteplase	2/1	16	38/M	Pons	Mannitol	5/0
6	48/F	Putamen	Mannitol	7/4	17	60/M	Cerebellum	Mannitol	5/1
7	64/M	Subcortex	Mannitol	1/0	18	71/M	Subcortex	Mannitol	1/0
8	77/M	Subcortex	Mannitol	2/0	19	69/F	Thalamus	Mannitol	7/5
9	49/M	Subcortex	Surgery	2/0	20	60/M	Subcortex	Mannitol	3/0
10	52/F	Putamen	Surgery	6/2	21	61/F	Putamen	Mannitol	11/6
11	89/F	Subcortex	Mannitol	6/0					